Manufacturing Constraint for deep drawn Sheet Metals in Density based Topology Optimization

Robert Dienemann[1]*, **Axel Schumacher**[2]

[1] *Altair Engineering, Cologne, Germany*
* *Corresponding author: dienemann@altair.de*
[2] *Chair for Optimization of Mechanical Structures, University of Wuppertal, Wuppertal, Germany*

Abstract
This contribution shows a scheme to optimize the shape and topology of deep drawn sheet metals. The density method on a voxel mesh is utilized and manufacturing constraints are applied to achieve uniform thick structures without undercuts in punch direction. Additionally, the manufacturing process is simulated in every iteration and the sheet metal structure is modified, such that no fractures occur during the deep drawing process.

Keywords: Topology Optimization, Manufacturing Constraint, Sheet Metal, Deep Drawing, Sensitivity

1. Introduction

Sheet metal parts are commonly applied lightweight structures incurring low manufacturing costs in mass production. A good design of sheet metal structures covers the mechanical requirements at prescribed load cases and the requirements of the manufacturing process.
In this contribution, the density method on a continuum mesh is chosen as approach for the topology optimization. It improves structures according to their sensitivities. To obtain sheet metal parts, new manufacturing constraints are implemented in the topology optimization. They allow for the optimization of sheet metal parts, which are manufactured by single-step deep drawing at room temperature. Therefore, the sensitivities of the objective function are manipulated for elements that are far away from the current mid-surface. Furthermore, manufacturing constraints for minimal draw radii and for the prevention of tearing during the deep drawing are implemented. In addition to the structural calculation with the prescribed load cases, a deep drawing simulation is performed. Its results are used to smooth the mid-surface in critical areas. These manufacturing constraints are realized as heuristics.

2. Deep Drawing

2.1 Manufacturing Process

Deep drawing is the tensile compression forming of a sheet metal blank into a hollow body (from DIN8584 [10]). Figure 1 shows the basic structure of deep drawing. The initially flat blank is formed by the relative movement of the punch in the direction of the die. In order to control the material flow of the sheet and to generate a tensile stress state at all points, the sheet is usually pressed onto the die by a blank holder.
Blank holders and dies often have draw beads in order to control the material flow of the sheet metal via the restraining force and to improve the effect of the blank-holder.

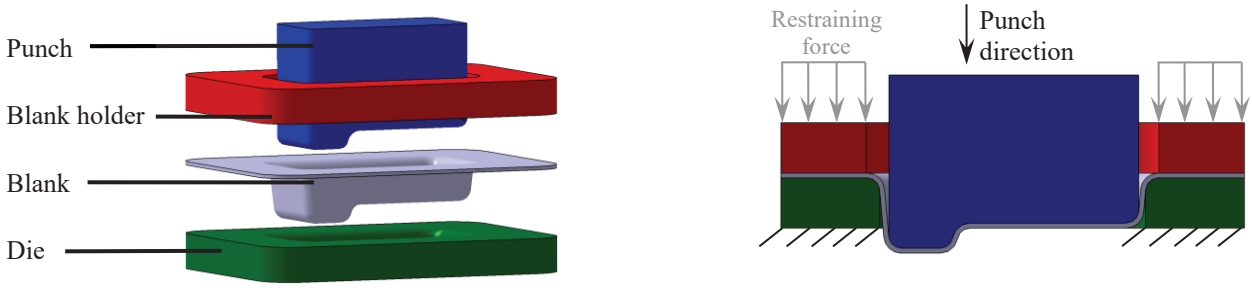

(a) Exploded view (b) Sectional view

Figure 1. Deep drawing – illustration

Figure 2 shows an exemplary cross-section of the formed component from Figure 1. In one production step, i.e. single-stage, only cross-sections without undercut in the direction of the punch can be produced as in Figure 2a. Geometries with an undercut in the punch direction as shown in Figure 2b can only be produced in several stages and are therefore not considered in this article.

(a) Without undercut (b) With undercut (shaded)

Figure 2. Manufacturability of a cross section

2.2 Evaluation Criteria

The results from the deep-drawing simulation are often evaluated using the forming limit diagram (FLD). The FLD depends on the material and the sheet thickness. Figure 3a shows an example of the FLD of the ductile cold forming steel DC04 at a thickness of 1 mm.

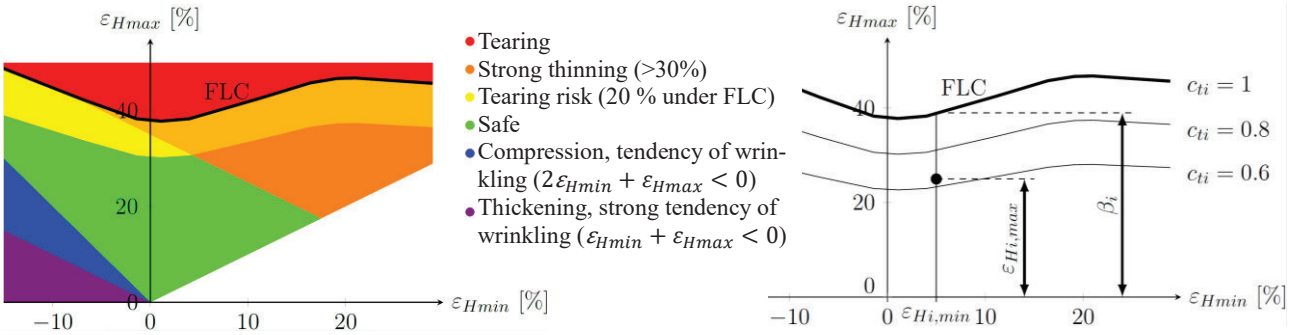

(a) FLD of DC04 with 1 mm thickness (b) Tearing criterion

Figure 3. Forming limit diagram and tearing criterion

For evaluation purposes, the principal strains in the shell ($\varepsilon_{Hi,max}$, $\varepsilon_{Hi,min}$) are calculated to predict the occurrence of tearing. The relevant curve for tearing is the forming limit curve (FLC). Above this curve the sheet cracks. A safety factor is often used to avoid the risk of tearing. This zone is shaded yellow in Figure 3a and has an exemplary vertical offset from the FLC of 20 %.

In order to identify tearing, the tearing criterion

$$c_{ti} = \frac{\varepsilon_{Hi,max}}{\beta_i} \tag{1}$$

for any location i is explained in Figure 3b. The black point in Figure 3b is the strain state at an exemplary location. The value β_i is the the maximum principal strain at which the FLC is reached with the same minimum principal strain $\varepsilon_{Hi,min}$. The tearing criterion c_{ti} describes the strain state of the element i in the FLD in relation to the FLC. At $c_{ti} = 1$ the strain state is on the FLC, at $c_{ti} < 1$ below. Therefore a design criterion can be that all tearing criteria must be smaller than a given value, for example $c_{ti} \leq 0.8$.

3. Optimization Approach

The density method [1] is applied on a voxel mesh. For material interpolation the SIMP-approach [15] is used. Stress as objective or constraint is handled as proposed by Le et al. [13]. Buckling safety from a linear buckling analysis can also be considered in the optimization task as described in Dienemann et al. [9].

The objective as well as the constraints can be a combination of the structural responses (volume, volume fraction, mass, compliance, von Mises stress, buckling safety, nodal displacement, eigenfrequency). The sensitivities of these responses are calculated analytically using the adjoint method. Based on the value and the sensitivities of the objective and constraints, separable convex approximations are generated (MMA, [14]) and solved by a dual optimizer [11, 5]. In order to prevent from checkerboarding a density filter is applied [3, 4], that maps the design variables $\mathbf{x}$ to the element densities $\tilde{\mathbf{x}}$ by averaging the design variables in a specified neigborhood of radius R. To save calculation time an element

deactivation and reactivation scheme is applied, that neglects minimum dense elements during the finite element calculation but allows for reactivation in subsequent iterations [8].

Figure 4 shows the optimization scheme with objective function f and constraints $\mathbf{g}$ for the optimization task

$$\min_{\mathbf{x}} f\left(\tilde{\mathbf{x}}(\mathbf{x})\right) \quad \mathbf{g}\left(\tilde{\mathbf{x}}(\mathbf{x})\right) \leq \mathbf{0}. \tag{2}$$

The basic scheme without manufacturing constraints is displayed in grey. The colored modifications are explained in the following chapters.

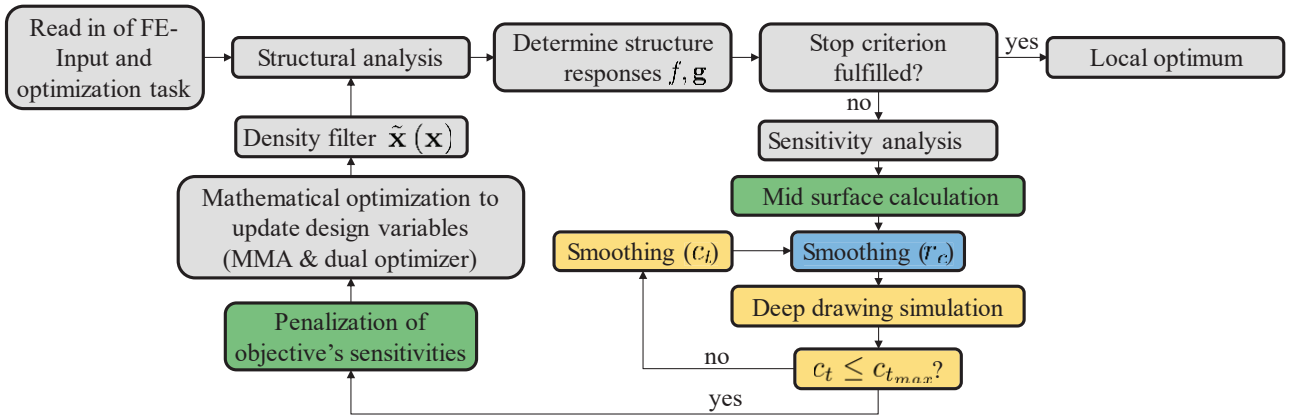

Figure 4. Optimization scheme – green: with manufacturing constraint for thin-walled structures without undercuts, blue: with manufacturing constraint on corner radius, orange: with manufacturing constraint on tearing criterion

4. Manufacturing Constraint for thin-walled Structures without Undercuts

The density method without manufacturing constraints usually yields structures, that cannot be manufactured economically in mass production. Therefore, in this chapter a manufacturing constraint is introduced to fulfill geometrical requirements of sheet metal components, that are deep drawn in one step.

The optimized geometry must fulfil the following geometrical criteria:

- Constant wall thickness
- No undercuts in punch direction
- No ribs.

For constant wall thickness, the change of wall thickness due to the manufacturing process is neglected. Ribs can only occur in punch direction if undercuts are avoided. In the following, the expansion in the punch direction is limited so that ribs are implicitly prevented.

4.1 Calculation of the Mid-Surface

To implement the manufacturing constraint, the mid-surface must be calculated from the position of the elements and their element density. For this purpose, the design space is divided into columns with width and depth w, which are oriented in punch direction (see Figure 5). Here, w denotes the element edge length of a voxel. An element is assigned to a column, if the element center is located inside the column. Within each column the mid-surface point is calculated from the weighted mean of the positions of the element midpoints ξ_i and the element density $\tilde{x}_i$:

$$\xi_{m_j} = \frac{\sum \xi_i(\tilde{x}_i - \tilde{x}_{min})}{\sum(\tilde{x}_i - \tilde{x}_{min})}. \tag{3}$$

The positions of the element centers are shown in Figure 5 exemplary for one column with grey arrows. Since elements with a minimum density should have no influence on the mid-surface position, the minimum density $\tilde{x}_{min}$ is subtracted from the element density $\tilde{x}_i$ in equation 3.

A mid-surface point is calculated for each column j. Between the column centers, the mid-surface area is interpolated linearly. Due to this averaging per column, the mid-surface cannot have any undercuts.

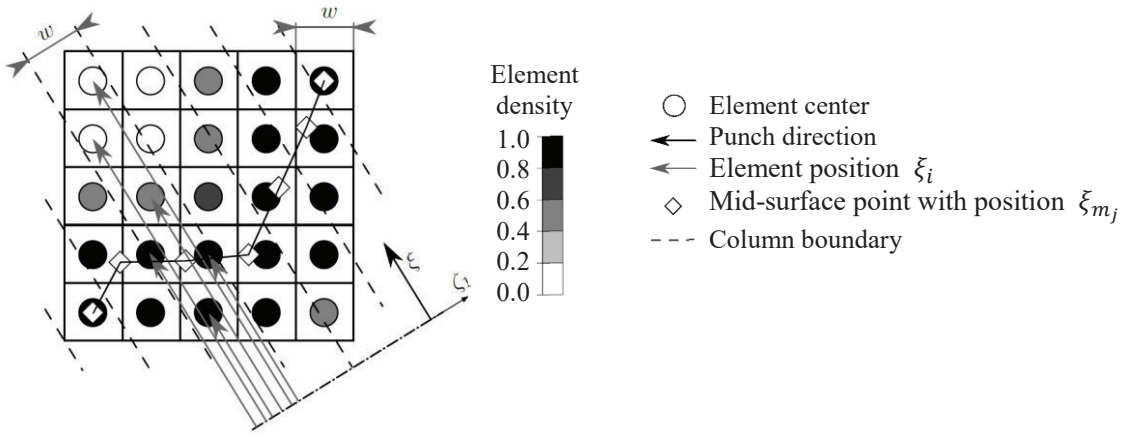

Figure 5. Mid-surface calculation on an exemplary cross section

4.2 Penalization of the Objective's Sensitivities far away from the Mid-Surface

The penalization of the sensitivities of the objective function is to be performed using the factor P_i. This penalization factor depends on the shortest distance d_i between the position $\mathbf{o}_i$ of the corresponding voxel center i and the mid-surface $\left[\zeta_{m_1}, \zeta_{m_2}, \xi_m\right]^T$ (considering the linear interpolation between the mid-surface points):

$$d_i = \min_j\left(\text{dist}\left(\mathbf{o}_i, \left[\zeta_{m_1 j} \quad \zeta_{m_2 j} \quad \xi_{mj}\right]\right)\right) = \min_j\left(\left|\mathbf{o}_i - \left[\zeta_{m_1 j} \quad \zeta_{m_2 j} \quad \xi_{mj}\right]^{\mathrm{T}}\right|\right). \tag{4}$$

The top resp. bottom side of the sheet structure is $\mathrm{d_i} = \frac{\mathrm{b_c}}{2}$ with the target wall thickness b_c. If the elements lie within the sheet ($d_i/b_c < 0.5$), the sensitivities of the objective function should remain unchanged ($P_i \approx 1$). If the elements are outside the shell structure ($d_i/b_c > 0.5$), the sensitivities of the objective function should be downgraded. For negative sensitivities (e.g. compliance), downgrading means multiplication by a small positive value ($\lim_{d_i/b_c \to \infty} P_i = 0$). In between, the penalization function should run continuously differentiable. These requirements are fulfilled by the penalty function

$$P_i(d_i) = \frac{1-\tanh(a[2d_i/b_c-1])}{1+\tanh(a)}. \tag{5}$$

shown in Figure 6. The parameter a describes the discreteness of the function. A low discreteness a causes an insufficient penalization and thus an unclear distinction between inside and outside the sheet. Consequently the shell structure represented by voxels can become locally considerably thicker than b_c. In contrast, a large discreteness a causes discontinuities in the optimization process, bad local minima and a slow relocation of the shell mid-surface. In all following examples $a = 4$ is used as compromise.

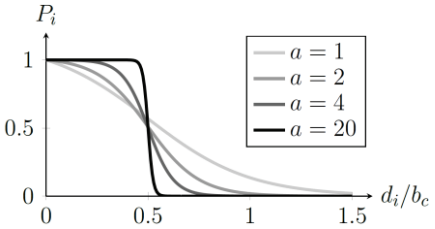

Figure 6. Mid-surface calculation on an exemplary cross section

If the sensitivities $\frac{\partial f}{\partial x_i}$ of the objective function f are negative, the sensitivity is worsened by multiplication by P_i. If they are positive, the sensitivity is downgraded by dividing by P_i. In the following, the objective function is limited to the compliance c and the volume v / volume fraction v_f or the mass m:

$$\frac{\partial \mathrm{f}}{\partial \mathrm{x_i}}' = \begin{cases} P_i \frac{\partial f}{\partial x_i}, & if\ f = x \\ \frac{1}{P_i}\frac{\partial f}{\partial x_i}, & if\ f = v, f = v_f\ or\ f = m. \end{cases} \tag{6}$$

The penalized sensitivities $\frac{\partial f}{\partial x_i}'$ are used for the update of design variables (see green part in Figure 4). Constraints can

be of any type and are not modified. This penalization is not differentiable as already the distance function in equation (4) is not differentiable. Hence this manufacturing constraint is not differentiable, but a heuristic, that relocates the mid-surface according to the sensitivities in the direction of the upper or lower surface of the sheet.
The penalization of the objective's sensitivities thus permits no undercuts and ensures maximum shell thickness. The filter radius, which should be selected as $R \approx 0.6 b_c$, ensures a minimum shell thickness. Some additional modifications improve the convergence behavior with this manufacturing constraint (e.g. alternating target wall thickness b_c, see [7]).

5. Consideration of Formability by Deep Drawing during the Optimization

As tearing often initiates at locations of strong curvature, a manufacturing constraint for minimum forming radii is introduced. It ensures, that all radii in the deep drawn sheet are greater than a user defined minimal forming radius: $r_c \geq r_{cmin}$.
The mid-surface, that was introduced in chapter 4.1 can be described as shell mesh, that has perfectly regular grids in the plane orthogonal to the punch direction. All mid-surface points have distance w to each other and are rectangularly arranged when projecting on that plane. Thus, the constraint on the forming radius can easily be applied as constraint on the angle between neighboring nodes in the mid-surface.
If the angle is larger than the critical one, the mid-surface is smoothed locally by filtering the ξ-coordinates of the mid-surface in a given neighborhood. This is done iteratively with an increasing neighborhood until the manufacturing constraint is satisfied. The smoothed surface is now used for the penalization of sensitivities in every iteration as shown in the blue part in Figure 4. Such also the element densities in the design space form a smoother sheet metal structure.

As the minimum corner radius does not guarantee, that no tearing occurs during the manufacturing process, additionally a manufacturing constraint on the tearing criteria is introduced: $c_t \leq c_{tmax}$. Therefore, deep drawing of the mid-surface is simulated in every iteration using the inverse approach. This is also known as OneStep-Solver (here Altair HyperForm and alternatively Autoform [12] were used). It is assumed, that the sheet metal is first deep drawn and afterwards the cut-outs are introduced. Therefore, the holes in the mid-surface are filled by linear interpolation.
Analogously to the minimum corner radius, now the mid-surface is smoothed locally in a neighborhood of tearing criteria, that are higher than the user defined maximum tearing criterion (see orange part in Figure 4). This is also done iteratively until the constraint on the tearing criterion is fulfilled in every iteration of the optimization loop.
More details on the implementation of the minimum corner radius and maximum tearing criterion are given in [6].

6. Examples

6.1 Quadratic Plate

The compliance of a quadratic plate is minimized at a volume fraction of $v_f \leq 7.5$ %. The force $F = 4$ kN is applied at the center of the design space (see Figure 7a). Voxels with an element edge length of $w = 0.5$ mm are used for discretization. The material is steel ($E = 210$ GPa, $\nu = 0.3$). A filter radius of $R = 1.2$ mm is used for the density filter. For the manufacturing constraint the target wall thickness is chosen as $b_c = 2$ mm and the punch direction is the opposite z-direction. As initial design with manufacturing constraint a flat plate is used, that is offset by 0.5 mm in z-direction from the middle of the design space. A symmetric flat plate as start design would be a local maximum and the sensitivities and top and bottom the same, so the mid-surface would not move. For deep drawing the material data of the high-strength complex-phase steel SZBS800 is used with a constant restraining of 0.25 all around the plate in Autoform, the friction factor is $\mu_0 = 0.15$.
The results are shown in Figure 7b-e. All compliance values are calculated for the full model. The more constraints are introduced, the higher is the compliance. The topology changes while the shape of the three sheet metal results is similar.

6.2 Control Arm

As industrial application a control arm is optimized. It is a part of the chassis and guides the wheel carrier in an almost vertical direction. The wishbone thus transmits lateral forces between the wheel and the body. The operating loads must be transmitted without exceeding the yield limit. In addition, the wishbone should buckle in a specified force corridor in the event of misuse loads. The buckling load must not be too high in order not to damage the body and not too low in order to fail as late as possible.

The design space is shown in Figure 8a with orange non-design space. The mass m is minimized with constraints on the maximum von-Mises stress σ_{vM} in 6 load cases and on the buckling safety in 3 linear buckling load cases. For the manufacturing constraint z is used as punch direction and $b_c = 3.8$ mm as target wall thickness.

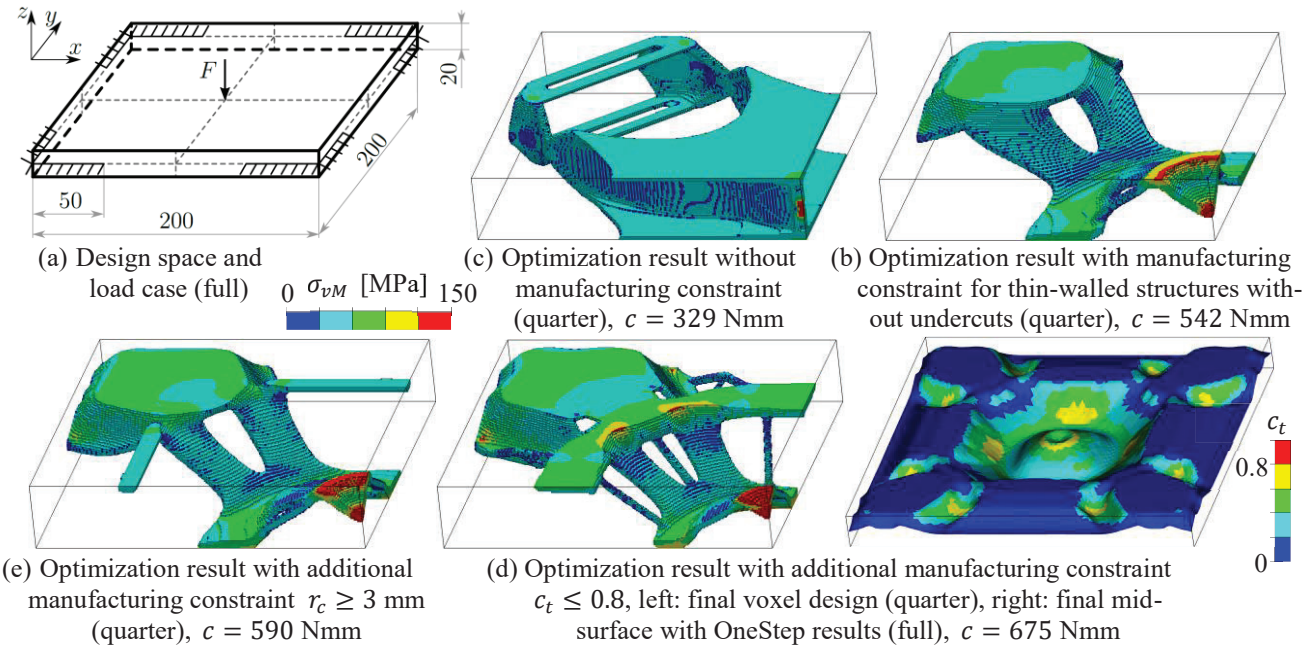

(a) Design space and load case (full)

(c) Optimization result without manufacturing constraint (quarter), $c = 329$ Nmm

(b) Optimization result with manufacturing constraint for thin-walled structures without undercuts (quarter), $c = 542$ Nmm

(e) Optimization result with additional manufacturing constraint $r_c \geq 3$ mm (quarter), $c = 590$ Nmm

(d) Optimization result with additional manufacturing constraint $c_t \leq 0.8$, left: final voxel design (quarter), right: final mid-surface with OneStep results (full), $c = 675$ Nmm

Figure 7. Quadratic Plate

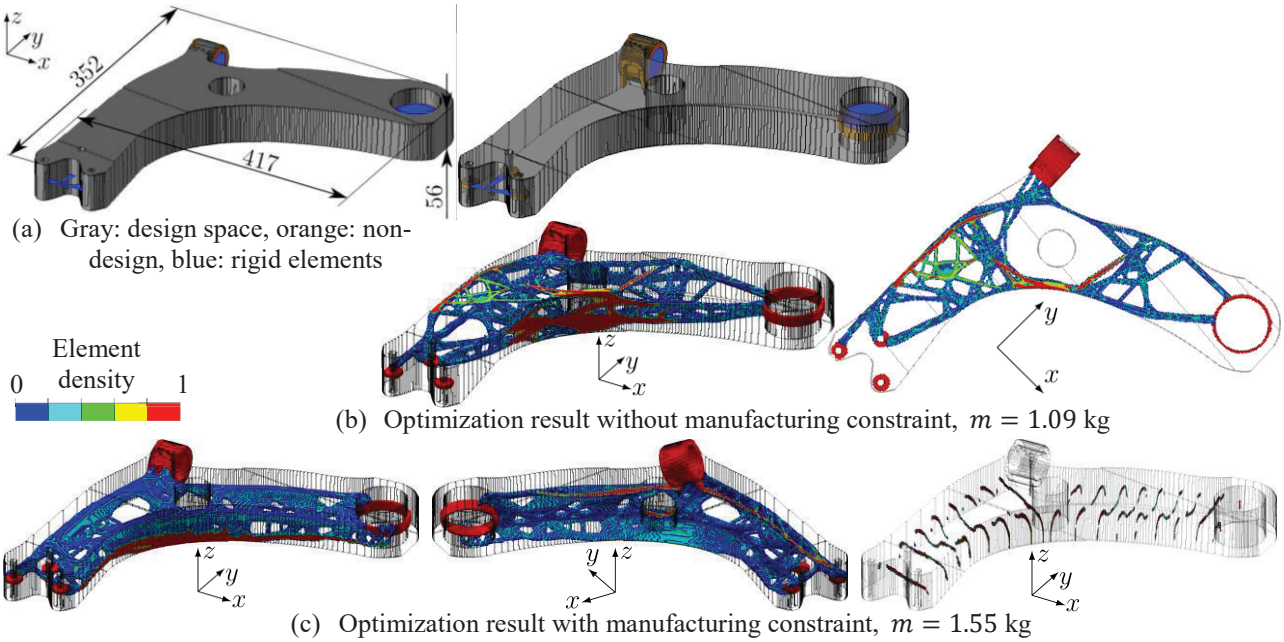

(a) Gray: design space, orange: non-design, blue: rigid elements

(b) Optimization result without manufacturing constraint, $m = 1.09$ kg

(c) Optimization result with manufacturing constraint, $m = 1.55$ kg

Figure 8. Control Arm, only elements with density > 0.1 displayed

7. Conclusions

This contribution shows a method for the topology and shape optimization of sheet metal components. Therefore heuristic manufacturing constraints are applied on the density method by manipulating the sensitivities of the objective function. Thereby a structure without undercuts and a prescribed wall thickness can be achieved, which fulfills a minimum corner radius and a maximum tearing criterion from a simplified deep drawing simulation, that is embedded the optimization.

References

1. Bendsøe MP, Sigmund O (2004) Topology Optimization: Theory, Methods and Applications. Springer, Berlin Heidelberg New York
2. Bletzinger K-U (2014) A consistent frame for sensitivity filtering and the vertex assigned morphing of optimal shape. Struct Multidiscip Optim 49: 873–895
3. Bourdin B (2001) Filters in topology optimization. Int J Numer Methods Eng 50: 2143–2158
4. Bruns TE, Tortorelli DA (2001) Topology optimization of non-linear elastic structures and compliant mechanisms. Comput Methods Appl Mech Eng 190: 3443–3459
5. Dienemann R, Schumacher A (2016) An efficient optimization method for mechanical shells considering cut-outs. Proc Appl Math Mech 16: 713–714
6. Dienemann R, Schumacher A, Fiebig S (2016) Topology and Shape Optimization of Sheet Metals with integrated Deep-Drawing-Simulation. In: Proceedings of the 12th World Congress on Computational Mechanics. Seoul, Korea
7. Dienemann R, Schumacher A, Fiebig S (2017) Topology optimization for finding shell structures manufactured by deep drawing. Struct Multidiscip Optim 56: 473–485
8. Dienemann R, Schumacher A, Fiebig S (2018) An Element Deactivation and Reactivation Scheme for the Topology Optimization Based on the Density Method. In: Advances in Structural and Multidisciplinary Optimization: Proceedings of the 12th World Congress of Structural and Multidisciplinary Optimization. Springer International Publishing: 1127–1142
9. Dienemann R, Schumacher A, Fiebig S (2018) Considering Linear Buckling for 3D Density Based Topology Optimization. In: EngOpt 2018: Proceedings of the 6th International Conference on Engineering Optimization, Lisbon, Portugal
10. DIN 8584 (2003) Fertigungsverfahren Zugdruckumformen - Teil 3: Tiefziehen; Einordnung, Unterteilung, Begriffe
11. Fleury C (1989) CONLIN: An efficient dual optimizer based on convex approximation concepts. Struct Optim 1: 81–89
12. Kubli W, Anderheggen E, Reissner J (1991) Nonlinear solver with uncoupled bending and stretching deformation for simulating thin sheet metal forming. VDI-Bericht 894: 325–343
13. Le C, Norato J, Bruns T, Ha C, Tortorelli D (2010) Stress-based topology optimization for continua. Struct Multidiscip Optim 41: 605–620
14. Svanberg K (1987) The method of moving asymptotes—a new method for structural optimization. Int J Numer Methods Eng 24: 359–373
15. Zhou M, Rozvany G (1991) The COC algorithm, Part II: Topological, geometrical and generalized shape optimization. Comput Methods Appl Mech Eng 89: 309–336